Applied Catalysis B: Environmental 192 (2016) 145–151

Contents lists available at ScienceDirect

Applied Catalysis B: Environmental

journal homepage: www.elsevier.com/locate/apcatb

Polymerizable complex synthesis of $SrTiO_3$:(Cr/Ta) photocatalysts to improve photocatalytic water splitting activity under visible light

Wei Chen [a], Heng Liu [a], Xiying Li [a], Shuang Liu [a], Li Gao [a], Liqun Mao [a], Zeyun Fan [b], Wenfeng Shangguan [b,*], Wenjian Fang [b,c], Yongsheng Liu [c]

[a] College of Chemistry and Chemical Engineering, Henan University, Kaifeng 475004, Henan, PR China
[b] Research Centre for Combustion and Environmental Technology, Shanghai Jiao Tong University, Shanghai 200240, PR China
[c] Institute of Solar Energy, Shanghai University of Electric Power, Shanghai 200090, PR China

ARTICLE INFO

Article history:
Received 31 December 2015
Received in revised form 16 March 2016
Accepted 24 March 2016
Available online 25 March 2016

Keywords:
Photocatalytic water splitting
Co-doping
Polymerizable complex synthesis
Z-scheme

ABSTRACT

Cr/Ta co-doped $SrTiO_3$ (STO:Cr/Ta) photocatalysts with high photocatalytic activity for water splitting under visible light have been synthesized by a polymerizable complex (PC) method. UV–vis diffuse reflectance spectra (DRS) showed that the Cr/Ta co-doping extended the absorption edge of STO to visible light region at the wavelength of 540 nm. Calculations based on density functional theory (DFT) indicated that, after doping, Cr 3d and O 2p orbits formed new impurity states within the forbidden gap of STO and facilitated the excitation of photons with low energy, as the Ta was mainly used to restrain the appearance of undesired Cr^{6+}. The photoelectrochemical measurements and XRD, SEM, BET analysis revealed that the excellent photocatalytic performance of photocatalyst prepared by a PC method was attributed to the high crystalline quality as well as relative large specific surface area. The photocatalytic activity of STO: (1% Cr/Ta) for H_2 evolution prepared by a PC method is 10 times higher than that of the sample prepared by a solid state reaction (SSR) method. The Pt/STO: (2% Cr/Ta) calcined at 1100 °C possessed the highest photocatalyitc activity for water splitting under visible light, thereby producing the average rate of H_2 evolution of 122.6 μmol h^{-1} (ca. 2.6% AYQ) measured at λ = 420 nm. Also, under a Z-scheme system, the Pt/STO: (2% Cr/Ta) exhibited AQY as high as 1.52% at λ = 420 nm for overall water splitting while Pt/WO_3 acting as an O_2 evolution photocatalyst.

1. Introduction

Photocatalytic water splitting has been considered as a promising method to generate clean energy H_2 directly from solar energy since the discovery of the Honda-Fujishima effect [1–3]. So far, although a large number of photocatalysts such as TiO_2 [4–6], $NaTaO_3$ [7–9], Ge_3N_4 [10], $K_2La_2Ti_3O_{10}$ [11], CdS [12–14], C_3N_4 [15–18] etc. have been explored for water splitting, most of them only response UV light (λ < 420 nm, 4% in the full solar energy) due to too wide energy gaps of semicondutors (E_g > 3.0 eV), which seriously restricts the efficiency of hydrogen production [19]. Therefore, the development of visible-light-driven photocatalysts is also a key task in this research field.

Generally speaking, metal oxide photocatalysts with large band-gap fail to absorb visible light due to deep energy level of O 2p orbits which mainly constitute valence band (VB) of photocatalysts. To obtain visible-light-driven photocatalysts, two strategies are used in the preparation of photocatalyic materials. First, S, N elements with stronger electron negativity than O are introduced into the formation of VB thus allowing narrower band gaps (e.g. TaON [20,21], Ta_3N_5 [22], GaN:ZnO [23]). Besides, metal ions doping also are used to extend the absorption spectra into the visible region, because the dopants assume mediators to decrease the band gaps of photocatalysts [24–26]. Nevertheless, considering the shortcoming of stability of (oxy)nitrides and (oxy)sulfides in photocatalytic reactions, metal ion doping is a very important method to develop the visible-light-driven photocatalysts.

$SrTiO_3$(STO) have been verified as one of the few promising materials that can split pure water into H_2 and O_2 [27]. However, STO can only respond to UV light due to its too large band gap (ca. 3.1 eV) [28,29]. It was reported doping Mn, Cr, Rh, Ir in STO extended the absorption spectra to 500–600 nm by forming impurity energy level near VB of STO [30,31]. Sayama et al. [32] first reported that Cr, Ta co-doping in STO could split water to either H_2 in the presence of methanol as a sacrificial reagent or stoichiometric H_2 and O_2 under a Z-scheme system under visible light, indicating

* Corresponding author.
E-mail address: shangguan@sjtu.edu.cn (W. Shangguan).

http://dx.doi.org/10.1016/j.apcatb.2016.03.057
0926-3373/

STO: (Cr/Ta) as a good candidate for photocatalytic water splitting under visible light. The STO: (Cr/Ta) exhibits robust stability, its photocatalytic activity is nonetheless relative low. Presumably, the low activity is ascribed to the lack of enough active sites related to the low specific surface area of photocatalysts after treatment under high temperature. It is well known that, both the specific surface area (corresponding to active sites) and crystalline quality (corresponding to the density of surface defect) of photocatalytic materials are two important factors to influence the photocatalytic activity [33]. The cooperation of large specific surface area and high crystalline quality facilitates the occurrence of photocatalytic reaction. Unfortunately, as the general method for the preparation of photocatalysts, conventional solid sate reaction (SSR) usually need high reaction temperature with long duration thus causing low surface area and the low photocatalytic activity. Recently, sol-gel hydrothermal [34–36], spray pyrolysis [37] and hydrothermal methods [38] have applied to respectively synthesize STO: Cr, STO: (Cr/Ta) and STO: (Sb/Rh) to enhance the photocatalytic activity by increasing the specific surface area of photocatalysts or inhibiting the formation of recombination centre of photogenerated electrons and holes, indicating the enhance of photocatalytic activity of STO: (Cr/Ta) by controlling its particle morphology and crystalline intensity.

Herein, we prepared co-doping visible-light-driven photocatalysts STO: (Cr/Ta) with relative large specific surface area and high crystalline quality by a PC method. The optimum reaction temperature and doping amounts were studied. The roles of doping ions in increasing the absorption of light and enhancing the photocatalytic activity were also investigated in light of density functional theory (DFT). Moreover, the photocatalytic performance of photocatalysts for overall water splitting was examined under a Z scheme system exposed to visible light.

2. Experimental

2.1. Material synthesis

The Cr/Ta co-doping STO was prepared by a PC method [39]. All materials were obtained from commercial sources and used without further purification. $TaCl_5$ was obtained from J&K Co. Ltd. and others from Sinopharm Chemical Reagent Co. Ltd. Typically, 80 mL methanol was used as a solvent to dissolve 5.11 g $TiC_{16}H_{36}O_4$. A large excess of citric acid CA, 19.9 g was added into the methanol solution with continuous stirring. After complete dissolution of the CA, 2.21 g $SrCO_3$, 0.062 g $Cr(NO_3)_3{\cdot}9H_2O$ and 0.053 g $TaCl_5$ were added to the solution. The mixture was then magnetically stirred for 1 h to afford a transparent solution and 30 mL ethylene glycol (EG) was added to this solution. Then, the solution was heated at 130 °C to promote esterification between EG and CA, yielding green-yellow resin. The resin was then calcined at 350 °C for 1 h to form black solid monolith. The resulting black powder was calcined on an Al_2O_3 plate at 650 °C for 2 h in air, then calcined at 900–1200 °C for 8 h to obtain 1% Cr and 1% Ta co-doping $SrTiO_3$, $SrTi_{0.98}Cr_{0.01}Ta_{0.01}O_3$ (denoted as STO: (1% Cr/Ta)). Additionally, to obtain 2–6% Cr/Ta co-doping STO samples, only appropriate amounts of $Cr(NO_3)_3{\cdot}9H_2O$ and $TaCl_5$ were added into the solution *via* the same synthesis route described above.

For a direct comparison, STO: (Cr/Ta) sample was synthesized *via* a SSR method reported by Kudo et al. [40]. stoichiometric amounts of $SrCO_3$, TiO_2, Cr_2O_3 and Ta_2O_5 were weighed and mixed with full grinding in a mortar. Then, the mixture was calcined in air at 1150 °C for 20 h.

2.2. Characterization

The crystal structure of the photocatalytic materials was confirmed by X-ray diffraction (Rigaku D/max-2200/PC Japan). The UV–vis diffuse reflection spectra (DRS) was determined by a UV–vis spectrophotometer UV-2450 (Shimadzu, Japan) and was converted to absorbance by the Kubelka–Munk method. The morphology of the samples was studied by scanning electron microscopy (FEI SIRION 200, USA). The specific areas of photocatalytic materials were determined by a BET method from N_2 absorption isotherms at 77 K (Micromeritics TriStarII3020 USA). The surface electronic state was analyzed by X-ray photoelectron spectroscopy (XPS, Shimadzu-Kratos, Axis UltraDLD, Japan). All the binding energy (BE) values were calibrated by using the standard BE value of contaminant carbon (C1s = 284.8 eV) as a reference.

2.3. Photoelectrochemical measurements

The photoelectrochemical measurements for photocurrent response were performed using a CHI660D electrochemical workstation with three-electrode system according to our previous report [41]. In this study, all potentials were converted into the potentials of reversible hydrogen electrode (RHE). The photocatalysts electrodes as the working electrodes were prepared by coating paste onto FTO glasses (15 $\Omega\,sq^{-1}$, transparency 84%, thickness 1.1 mm) with an area of 1 cm × 2 cm. The working electrodes were prepared as follow: 6 mg ground powder was immersed into mixed solution containing 10 μL acetylacetone, 10 μL Triton 100 and 300 μL distilled water to obtain viscous slurry. The slurry was then injected onto FTO glass and was calcined in air at 350 °C for 1 h. Measurements were performed using a quartz electrochemical cell with a Pt wire as a counter electrode and an Ag/AgCl as a reference electrode. Current–time curves were measured in a 0.1 M KOH aqueous solution as a supporting electrolyte. A 300 W Xenon lamp with a 420 nm cutoff was used as a light source. The effective surface area of the electrodes was 1 cm × 1.5 cm.

2.4. Calculation

The energy bands and density of states (DOS) were calculated by using the standard CASTEP package based on the density functional theory (DFT). Perdew–Burke–Ernzerh (PBE) was used the correlation. The cutoff energy was selected at 500 eV and 4 × 4 × 4 *k*-points for samples were chosen in the calculation. During the geometry optimization, the parameters of convergence criteria were set as: energy tolerance 5×10^{-6} eV per atom, max. force 0.01 eV per Å, max. stress 0.02 GPa, max. displacement 5×10^{-4} eV Å.

2.5. Photocatalytic reactions

Photocatalytic reactions for water splitting were carried out in a 350 mL top irradiation reaction quartz cell at room temperature. The catalyst powder (0.1 g) was suspended in 65 mL methanol solution(10 vol%) containing a certain amount of H_2PtCl_6 under magnetic stirring. The reaction cell was connected to a vacuum system, and a 300 W Xe lamp with a cut-off filter to remove UV light ($\lambda < 420$ nm) was used as a light source. At initial stage, Pt species were gradually deposited and loaded on the surface of photocatalysts. After reaction, 0.3 wt% Pt/STO: (Cr/Ta) was filtered and dried at 60 °C for 2 h as a H_2 evolution photocatalyst for Z-Scheme water splitting reaction. The Z-Scheme water splitting reaction was performed in the same system. 0.05 g 0.3% wt Pt/STO: (Cr/Ta) as a H_2 evolution photocatalyst and 0.05 g 0.5% wt Pt/WO_3 as an O_2 evolution photocatalyst were suspended in 65 mL NaI aqueous solution (5 mmol/L). The gases evolved were analyzed by GC with a TCD detector (Huaai, GC9560, China, MS-5A, argon as carrier gas).

The apparent quantum yield (AQY) for water splitting was measured using the same setup. The AQY was calculated under irradiation light at λ = 420 nm using a band-pass filter (λ = 420 ± 5 nm), according to equations given below:

$$\mathrm{AQY}(\%) = \frac{\text{The rate of reacted electrons}}{\text{The rate of incident photons}} \times 100$$

$$= \frac{\text{The rate of evolved } H_2 \text{ molecules} \times A}{\text{The rate of incident photons}} \times 100$$

A = 2 for half reaction or 4 for Z-scheme system

The number of incident photons was measured using a Si photodiode.

3. Results and discussion

3.1. Crystalline structures, morphologies and BET

The XRD patterns of STO (1% Cr/Ta) samples prepared under different temperatures by a PC method are shown in Fig. 1, while the counterpart of STO: (1% Cr/Ta) sample was prepared by a SSR method. As shown in Fig. 1, all STO: (Cr/Ta) samples exhibit the same phase as STO with a cubic structure (PDF 35-0734), and impurity phases, especially Cr or Ta oxides, are not observed, indicating that Cr, Ta probably doped into the crystal lattice of STO. There are no any changes of main diffraction peaks of crystal faces derived from the distortion of unit cell after doping. This reason presumably lies in the fact that the radium of Cr (0.062 nm) and Ta (0.064 nm) is close to that of Ti (0.061 nm). Of note, the diffraction peaks of XRD become sharp as calcination temperatures rise, suggesting that the crystallization of STO: (Cr/Ta) proceeds gradually with increasing the calcination temperature.

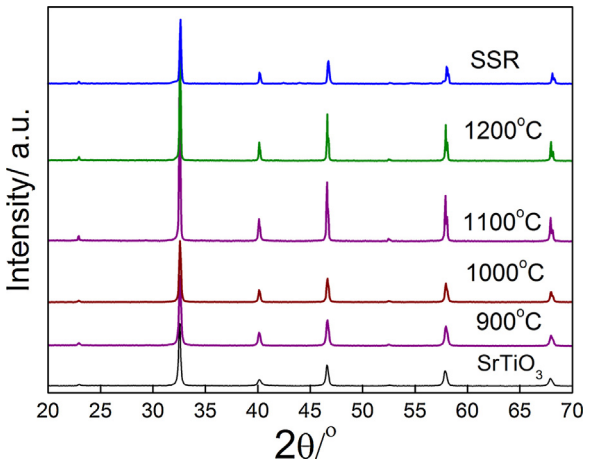

Fig. 1. XRD patterns of STO and 1% Cr, Ta co-doping STO prepared by a PC method under different temperatures.

Fig. 2 shows the SEM images of STO: (1% Cr/Ta) samples prepared at different calcination temperatures. Well-crystallized particles of all samples are observed regardless of the calcination temperatures, whereas the particle sizes of as-prepared samples become larger and more regular with increasing calcination temperature. This result is in agreement with the XRD measurements, in which the diffraction peaks become narrower and stronger. The specific surface areas of photocatalytic materials, as shown in Table 1, decrease with the increase of calcination temperatures. This result is further validated by the SEM measurements, in which the size of particles increases from about 80–300 nm corresponding to the specific surface areas decreasing from 6.65-1.06 $m^2\ g^{-1}$. Additionally, the low specific surface area (ca. 0.34 $m^2\ g^{-1}$) of the STO: (Cr/Ta) sample

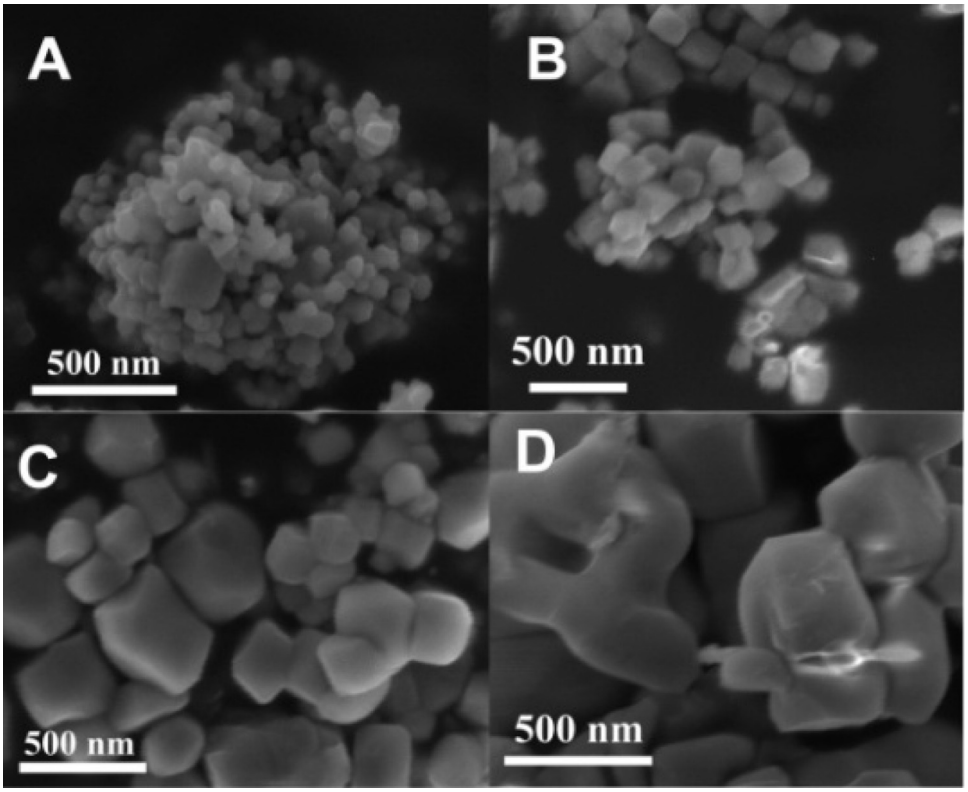

Fig. 2. SEM images of STO: (1%Cr/Ta) prepared at different calcination temperatures for 8 h by a PC method, 1000 °C (A), 1100 °C (B), (C)1200 °C and by SSR (D) (1150 °C for 20 h).

Table 1
Physicochemical properties and photocatalytic performance of undoped STO and Cr/Ta co-doped STO.

Temperature of calcinations/°C	Amount of dopant (%)	SBET ($m^2 g^{-1}$)	H_2 evolution rate[a] ($\mu mol\ h^{-1}$)	AQY(%)@420 nm
1000	0	2.72	trace	–
900	1	9.78	11.6	–
1000	1	6.65	16.8	–
1100	1	2.86	38.9	0.97
1150	1	1.99	35.3	0.83
1200	1	1.08	10.0	–
1150 (SSR)[b]	1	0.34	3.8	–
1100	2	3.1	122.6	2.6
1100	3	4.38	0.65	–
1100	4	3.92	0.40	–

Photocatalytic reaction conditions: 0.1 g catalyst, 300 W Xe lamp (λ >420 nm), 65 mL methanol solution (10 vol%), 0.3% Pt loading.
[a] Average H_2 evolution rates in 3 h after reaction 15 h.
[b] Prepared at 1150 °C for 20 h.

prepared by a SSR method, which is attributed to the high reaction temperature (1150 °C) and long reaction time (20 h).

3.2. Optical and photoelectrochemical properties

The DRS of STO: (1% Cr/Ta) samples and undoped one are shown in Fig. 3. The results demonstrate that undoped STO only responds to the UV light with wavelength shorter than ca. 390 nm, corresponding to band gap of ca. 3.2 eV. However, the absorption edges of STO: (Cr/Ta) samples extend to visible light at the wavelength 540 nm, which corresponds to band gap of ca 2.3 eV. As reported [42], absorption edges of Ta_2O_5 and Cr_2O_3 are at 310 and 360 nm, respectively. As a result, Cr and Ta have been doped in crystal lattice instead of being loaded on the surface of STO. The narrow band gap (2.3 eV) should originate from the transition from the doping energy level to conduction band (CB) rather than VB to CB of STO. In addition, with exception of the intrinsic band gap absorption, the weak absorption at a range of 540–800 nm is also seen from Fig. 3, in which the absorption bands from 540 to 700 nm should be ascribed to the d–d transition of Cr^{3+} and the absorption bands from 700 to 800 nm probably be attribute to oxygen vacancy states [42].

To further investigate the doping effects of Cr, Ta on the electronic structure of STO, the density of states (DOS) of pure STO, Ta doped STO (STO: Ta) and STO: (Cr/Ta) were calculated and the results were shown in Fig. 4. From Fig. 4a, the computed band gap of pure STO is ca. 1.83 eV, in agreement with previous calculated value, which is narrower than the experimental value (ca. 3.2 eV) due to the well-known limitation of calculation method [43,44]. The

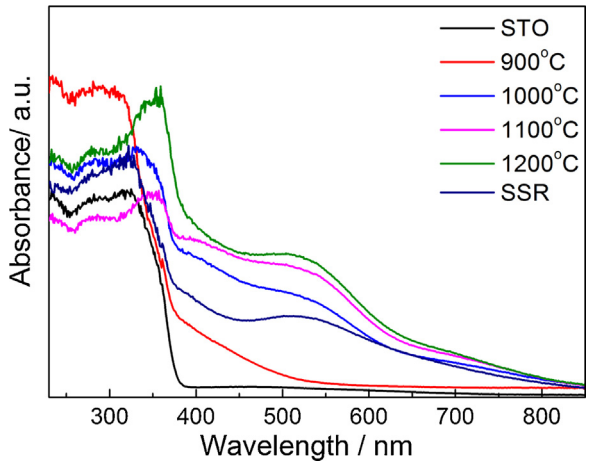

Fig. 3. UV–vis DRS of undoped and STO: (1% Cr/Ta) prepared at different calcination temperatures for 8 h.

PDOS of STO show that the VB maximum (VBM) is composed of O 2p, while the CB minimum (CBM) is mainly consist of Ti 3d along with a little contribution of O 2p. The Sr element is not involved in energy bands but the pervoskite structure. The PDOS of STO: Ta is showed in Fig. 4b. Given that the ion radium of Ta^{5+} (0.064 nm) is closer to that of Ti^{4+} (0.061 nm) compared to the ion radium of Sr^{2+} (0.144 nm), the Ta doping calculation was carried out by introducing Ta into Ti lattice sites. From Fig. 4b, in contrast to pure STO, the band gap and position of VBM and CBM of STO: Ta have no change, although the Ta 5d orbit participates in the formation of CB. However, for STO: (Cr/Ta), the PDOS show (Fig. 4c) that some new impurity states are formed by Cr 3d and O 2p orbits between VBM and CBM, although the band gap and position of VBM and CBM are very similar to that of STO: Ta. These results indicate that the red shift of absorption edge of STO after co-doping referring to DRS arises from the impurity states above the VBM, thereby reducing the band gap about 1.0 eV. Thus, the visible light photons can excite the electrons from the occupied Cr 3d to unoccupied Ti 3d which subsequently reduce H^+ to H_2 in the photocatalytic water splitting process. Moreover, the Ta doping inhibits the appearance of Cr^{6+} as the centre of charge recombination, since once the low valence Cr^{3+} replaces the high valence Ti^{4+}, Cr^{6+} is more likely to emerge in order to balance charge [45].

3.3. Photocatalytic water splitting activities

The Table 1 shows the hydrogen evolution rates of photocatalysts with 0.3 wt% Pt loading. The reaction was performed in the methanol solution containing 0.1 g catalyst under visible light (λ > 420 nm). STO have no photocatalytic activity because its band gap is too wide to respond to visible light. STO: (Cr/Ta) photocatalysts ensure splitting water into hydrogen under visible light due to the appearance of impurity energy level within the forbidden gap of STO. It is noteworthy that, with the increase of the calcination temperatures below 1100 °C, the rates of photocatalytic hydrogen evolution on STO: (1% Cr/Ta) samples increased even though the specific surface areas decreased gradually. The highest hydrogen evolution rate was up to 38.9 $\mu mol\ h^{-1}$ with AQY of ca. 0.97% when the calcination temperature was 1100 °C, even 10 times as that on the STO: (1% Cr/Ta) sample prepared by SSR (3.8 $\mu mol\ h^{-1}$). Nevertheless, a further increase of calcination temperatures would lead to decrease in photocatalytic hydrogen production. According to the previous results [33], the photocatalytic activity of photocatalyst for water splitting is influenced intensively by crystalline quality as well as specific surface areas. The high crystalline quality and large specific surface area facilitate the photocatalytic reaction for hydrogen evolution. Under low temperature (900 °C), although the specific surface area is large, the crystalline quality is relatively low and results in many crystal defects, which act as recombination centre of photogenerated carriers and cause the reduction of pho-

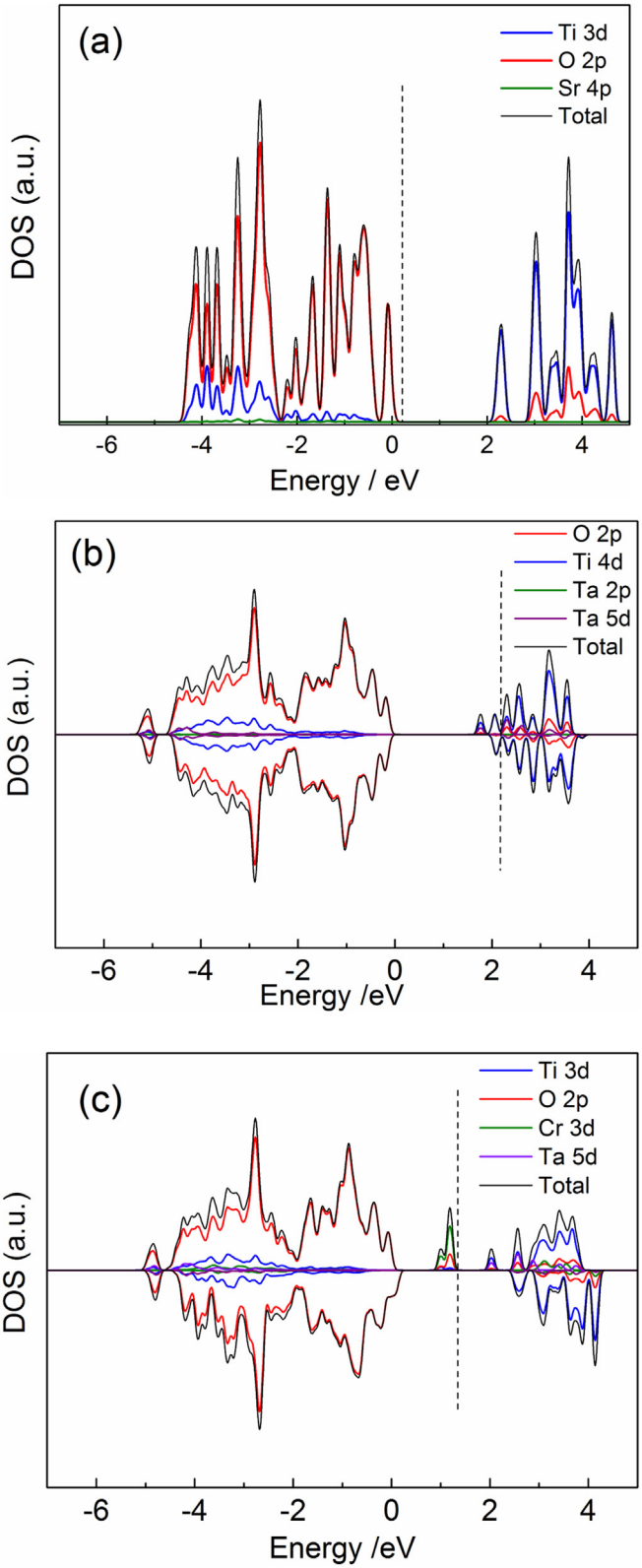

Fig. 4. The calculated density of states (DOS) of STO(a), Ta doped STO (b) and Cr-Ta co-doped STO(c). The vertical dashed lines indicate the Fermi level.

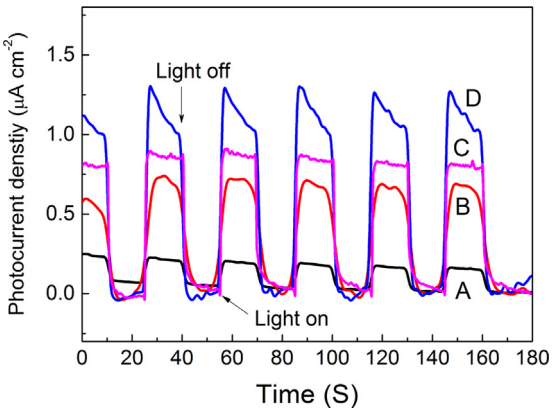

Fig. 5. Current–time curves of STO (1% Cr/Ta) prepared by a PC method at 1000 °C (A), 1100 °C (B), prepared by SSR (C) and of STO (2% Cr/Ta) prepared by a PC method at 1100 °C (D) under intermittent irradiation (λ > 420 nm) in a 0.1 M KOH solution, potential 1.44 V vs RHE.

tocatalytic activity [46]. In contrast, if the calcination temperature is high, the crystalline quality is good, but the specific surface area is low and results in poor photocatalytic activity due to the lack of active sites for hydrogen evolution. In the case of STO: (Cr/Ta) sample prepared by SSR, its photocatalytic hydrogen evolution rate is only 3.8 μmol h^{-1} due to too low specific surface area (0.34 m^2 g^{-1}), although the crystalline quality is very high.

To examine the influence of crystalline quality on the separation of photogenerated electrons and holes, the photocurrent response curves for STO: (Cr/Ta)-based electrodes under intermittent irradiation (λ > 420 nm) were carried out. The current-time curves (Fig. 5) show that the STO: (Cr/Ta) sample synthesized by a PC method at 1100 °C (Fig. 5c) provides stronger photocurrent than the STO: (Cr/Ta) sample synthesized at 1000 °C (Fig. 5b), confirming that high crystalline quality (low defect density) is a positive factor for separating the photoinduced carriers [47]. Additionally, although the photocurrent intensity of the STO: (1% Cr/Ta) synthesized by a PC method at 1100 °C is somewhat larger than that of STO: (1% Cr/Ta) by a SSR method, the photocatalytic activity for hydrogen evolution of STO: (1% Cr/Ta) (PC, 1100 °C) is apparently higher than that of STO: (Cr/Ta) (SSR), indicating that specific surface areas of samples will become a key factor for influencing the photocatalytic activity when the defect density is relative low.

It is noteworthy that, at initial stage, none of photocatalysts in this study had high photocatalytic activity for hydrogen evolution regardless of preparation conditions. To investigate the influence of dopants on delaying hydrogen evolution, the chemical states of Ta, Cr in STO: (1% Cr/Ta) samples prepared at 1000 °C and 1100 °C before and after reaction were measured by XPS (Fig. 6). As shown in Fig. 6, Cr $2p_{3/2}$ XPS spectra of all samples display broad peaks and have been fitted to two overlapped peaks at ca. 576.7 eV and 579.3 eV, which are attributed to Cr^{3+} and Cr^{6+} [40,48], respectively. In comparison to before reaction, after reaction, the amount of Cr^{6+} decreases apparently, suggesting that the low activity of photocatalysts at initial stage is because photogenerated electrons were consumed for the reduction of Cr^{6+} to Cr^{3+} instead of H^+ to H_2. The Ta $5d_{7/2}$ spectra peaks locate at ca. 25.5 eV assigned as Ta^{5+} [49], which inhibits the formation of undesired Cr^{6+} or defects. In addition, the ratio of Cr^{6+}/Cr^{3+} of the STO: (1% Cr/Ta) prepared at 1100 °C is closed to that of the STO: (1% Cr/Ta) prepared at 1000 °C, although the photocatalytic activity of the former is higher apparently than that of the latter, indicting the distinction of activity of photocatalysts prepared at different calcination temperatures originates from the crystalline quality mentioned above rather than chemical states of dopants.

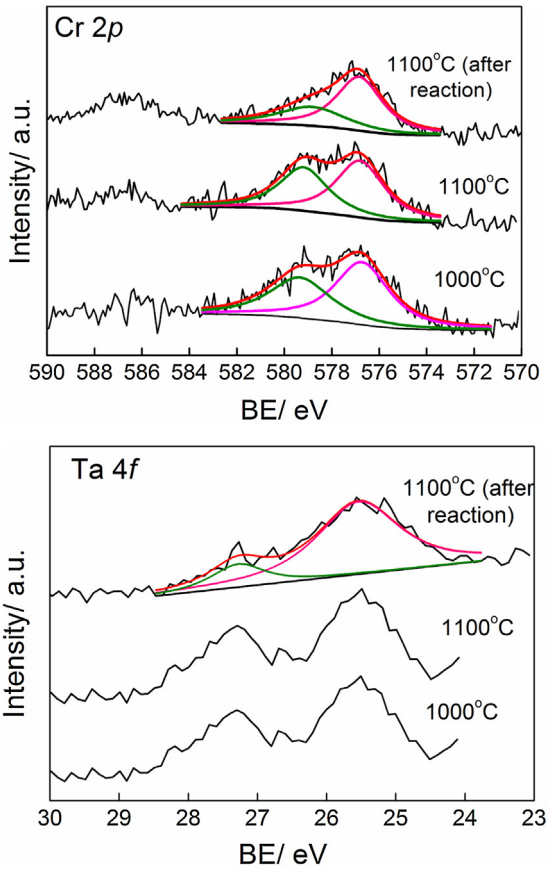

Fig. 6. XPS spectra for STO (1% Cr/Ta) prepared by a PC method at 1000 °C, 1100 °C and 1100 °C after reaction 15 h.

3.4. Optimizing of doping and loading amounts

In general, doping ions not only form the impurity energy level in the forbidden bands of photocatalysts, but act as the combination centre of photoinduced carriers [50]. Therefore, with the ambivalent influence on absorption light and separation of charge carriers, doping amounts have optimal values. Fig. 7 shows the XRD patterns of STO: (Cr/Ta) samples with different doping amounts. From Fig. 7, there are no noticeable changes regardless of doping amounts. In addition, the impurity phase of Cr or Ta oxides was not detected even if the doping amounts was up to 6%, further addressing that the Cr and Ta doped into the crystal lattice of STO indeed.

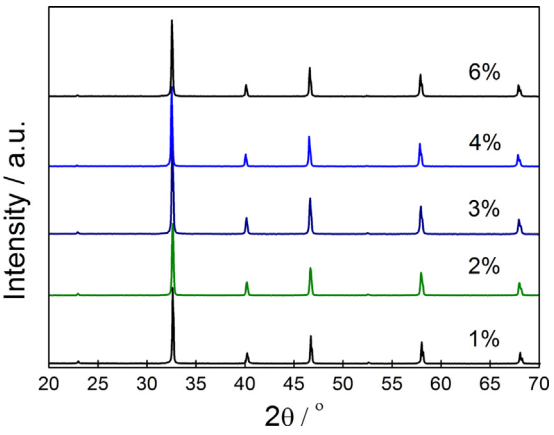

Fig. 7. XRD patterns of STO(Cr/Ta) with different doping amounts prepared by a PC method.

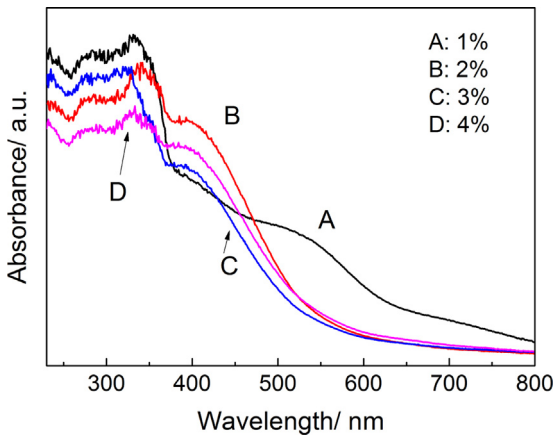

Fig. 8. UV–vis DRS of STO(Cr/Ta) with different doping amounts prepared by a PC method.

Also, there are negligible changes of absorption edges (ca. 550 nm) with the increase of doping amounts (Fig. 8). However, it is definite that 2–4% doped STO samples display little absorption in the range of 550–800 nm. The result indicates that under high Ta doping amounts conditions, the Cr^{6+} and defect are inhibited very well and cause the weaker d–d transition of Cr and less oxygen vacancy density.

The photocatalytic H_2 evolution rates of STO with different doping amounts (Table 1) display that the optimum doping amount is 2%, reaching 122.6 μmol h^{-1} with ca. 2.6% AQY at λ = 420 nm. Nevertheless, excessive doping amounts will lead to the rapid inactivation of photocatalysts. For instance, the H_2 evolution rate of STO: (3% Cr/Ta) is only 0.65 μmol h^{-1}. This reason is that low doping amounts is essentially related to of the deficiency of photoinduced carriers and excessive doping amounts nonetheless usually cause the strong recombination of photogenerated electrons and holes. Additionally, Ta doping with proper amounts also restrains the generation of oxygen vacancy which acts as recombination centre, thus enhancing the photocatalytic activity. Compared to 1% doping, 2% doping shows the stronger photocurrent intensity (Fig. 5C, D) demonstrating its good performance in separating electron and hole pairs and sufficient photoinduced carriers (Table 1).

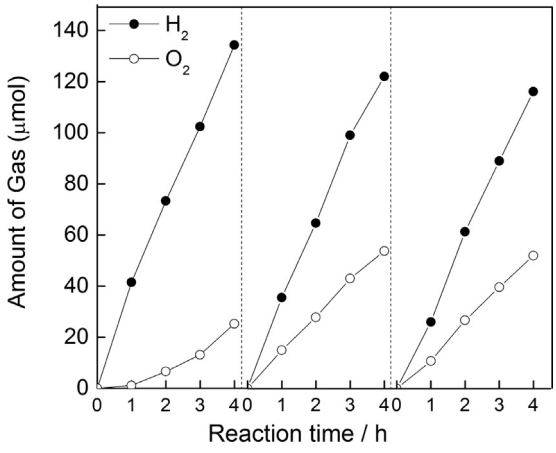

Fig. 9. Photocatalytic activity under a Z-scheme system for overall water splitting using 0.3% Pt/STO (2% Cr/Ta) and 0.5% Pt/WO_3. Reaction conditions: 0.05 g of each, 300 W Xe lamp (λ > 420 nm), 65 mL 5 mM NaI aqueous solution.

3.5. Water splitting under visible light over a Z-scheme system

It has been reported [51] that STO: (Cr/Ta) can achieve overall water splitting under a two-step water splitting (Z-scheme) system. To investigate the photocatalytic activity of STO: (Cr/Ta) photocatalysts prepared by a PC method under visible light ($\lambda > 420$ nm) for overall water splitting, the time course of H_2 and O_2 evolution is shown in Fig. 9 for a mixture of 0.3 wt% Pt/STO: (2% Cr/Ta) as a H_2 evolution photocatalyst and 0.5 wt% Pt/WO_3 as an O_2 evolution photocatalyst. At the initial stage of the reaction (in the first 4 h run), the ratio of H_2/O_2 is apparent larger than that in stoichiometry from water. This may be ascribed to the high concentration of I^- in the reaction solution at the initial reaction stage, during which the holes from VB of Pt/WO_3 are mainly used to oxide I^- to IO_3^- instead of OH^- to O_2. As the reaction proceeds, the ratio of H_2/O_2 is gradually close to stoichiometic value and subsequently reaches the dynamic stable stage (in the second 4 h run), in which the electrons of Pt/STO: (Cr/Ta) reduce H^+ to H_2 and holes oxide I^- to IO_3^- while the electrons of Pt/WO_3 reduce IO_3^- to I^- and holes oxide OH^- to O_2. The average rates of H_2 and O_2 at stable states are 30.5 μmol h^{-1} and 13.5 μmol h^{-1}, respectively, and the ratio of H_2/O_2 is 2.26, which is close to the exact stoichiometry of water splitting. Also, the AQY is estimated to be ca. 1.52% at 420 nm based on the H_2 evolution rate.

4. Conclusions

In summary, STO: (Cr/Ta) photocatalysts with high photocatalytic activity for water splitting under visible light have been synthesized by a PC method. After doping, the formation of new impurity energy level by Cr 3d and O 2p orbits endow the STO with visible-light-responsive property. The photocatalytic activity for H_2 evolution of STO doped 1% Cr and Ta prepared by a PC method is 10 times higher than that of sample prepared by a SSR method. The good photocatalytic performance is attributed to the high crystalline quality as well as relative large specific area of photocatalyst, which not only reduce the combination of photoincuced carriers but also afford sufficient active sites for water splitting. The STO: (2% Cr/Ta) possesses the highest photocatalytic activity for water splitting under visible light, and the average rate of H_2 evolution is 122.6 μmol h^{-1} with ca. 2.6% AYQ at $\lambda = 420$ nm. Under a Z-scheme system, Pt/STO: (2% Cr/Ta) also exhibit AQY as high as 1.52% at $\lambda = 420$ nm for overall water splitting when Pt/WO_3 as an O_2 evolution photocatalyst. The results suggest that it is a simple and effective method to obtain doped photocatalysts for improving photocatalytic water splitting activity.

Acknowledgements

This work was supported by the National High Technology Research and Development Program of China (2012AA051501), the International Cooperation Project of Shanghai Municipal Science and Technology Commission (12160705700) and the International Cooperation Project of Department of Science and Technology of Henan Province (162102410011).

References

[1] X. Chen, S. Shen, L. Guo, S. Mao, Chem. Rev. 110 (2010) 6503–6570.
[2] X. Li, J. Yu, J. Low, Y. Fang, J. Xiao, X. Chen, J. Mater. Chem. A 23 (2015) 2485–2543.
[3] A. Fujishima, K. Honda, Nature 238 (1972) 37–38.
[4] Y. Ma, X. Wang, Y. Jia, X. Chen, H. Han, C. Li, Chem. Rev. 114 (2014) 9987–10043.
[5] Y. Huo, X. Yang, J. Zhu, H. Li, Appl. Catal. B 106 (2011) 69–75.
[6] E. Cui, G. Lu, Int. J. Hydrogen Energy 39 (2014) 8959–8968.
[7] A. Iwase, H. Kato, A. Kudo, Appl. Catal. B 136–137 (2013) 89–93.
[8] J. Sun, G. Chen, Y. Li, R. Jin, J. Pei, Energy Environ. Sci. 4 (2011) 4052–4060.
[9] P. Zhang, J. Zhang, J. Gong, Chem. Soc. Rev. 43 (2014) 4395–4422.
[10] J. Sato, N. Saito, Y. Yamada, K. Maeda, T. Takata, J. Kondo, M. Hara, H. Kobayashi, K. Domen, Y. Inoue, J. Am. Chem. Soc. 127 (2005) 4150–4151.
[11] C. Thaminimulla, T. Takata, M. Hara, J.N. Kondo, K. Domen, J. Catal. 196 (2) (2000) 362–365.
[12] S. Chen, X. Chen, Q. Jiang, J. Yan, C. Lin, W. Shangguan, Appl. Surf. Sci. 316 (2014) 590–594.
[13] H. Yan, J. Yang, G. Ma, G. Wu, X. Zong, Z. Lei, J. Shi, J. Catal. 266 (2009) 165–168.
[14] Y. Yu, G. Chen, L. Hao, Y. Zhou, Y. Wang, J. Pei, J. Sun, Z. Han, Chem. Commun. 49 (2013) 10142–10144.
[15] Q. Li, B. Guo, J. Yu, J. Ran, B. Zhang, H. Yan, J. Gong, J. Am. Chem. Soc. 133 (2011) 10878–10884.
[16] X. Wang, K. Maeda, A. Thomas, K. Takanabe, G. Xin, J. Carlsson, K. Domen, M. Antonietti, Nat. Mater. 8 (2009) 76–80.
[17] Q. Xiang, J. Yu, M. Jaroniec, J. Phys. Chem. C 115 (2011) 7355–7363.
[18] B. Chai, T. Peng, J. Mao, K. Li, L. Zan, Chem. Chem. Phys. 14 (2012) 16745–16752.
[19] K. Maeda, K. Domen, J. Phys. Chem. Lett. 1 (2010) 2655–2661.
[20] M. Hara, J. Nunoshige, T. Takata, J. Kondo, K. Domen, Chem. Commun. 49 (2003) 10142–10144.
[21] W. Chen, M. Chu, L. Gao, L. Mao, J. Yuan, W. Shangguan, App. Surf. Sci. 324 (2015) 432–437.
[22] Z. Wang, J. Hou, C. Yang, S. Jiao, K. Huang, H. Zhu, Energy Environ. Sci. 6 (2013) 2134–2144.
[23] K. Maeda, T. Takata, M. Hara, N. Saito, Y. Inoue, H. Kobayashi, K. Domen, J. Am. Chem. Soc. 127 (2005) 8286–8287.
[24] D. Hwang, H. Kim, J. Jang, S. Bae, S. Ji, J. Lee, Catal. Today 93–95 (2004) 845–880.
[25] W. Li, X. Liu, H. Li, J. Mater. Chem. A 3 (2015) 15214–15224.
[26] M. Nasir, J. Zhang, F. Chen, B. Tian, Res. Chem. Intermed. 41 (2015) 1607–1624.
[27] B. Wang, S. Shen, L. Guo, Appl. Catal. B 166 (2015) 320–326.
[28] T. Townsend, N. Browning, F. Osterloh, Energy Environ. Sci. 5 (2012) 9543–9550.
[29] J. Luo, P. Maggard, Adv. Mater. 18 (2006) 514–517.
[30] R. Konta, T. Ishii, H. Kato, A. Kudo, J. Phys. Chem. B 108 (2004) 8992–8995.
[31] P. Shen, J. Lofaro Jr., W. Woerner, M. White, D. Su, A. Orlov, Chem. Eng. J. 223 (2013) 200–208.
[32] K. Sayama, K. Mukasa, R. Abe, Y. Abe, H. Arakawa, Chem. Commun. (2001) 2416–2417.
[33] A. Kudo, Y. Miseki, Chem. Soc. Rev. 38 (2009) 253–278.
[34] H. Yu, S. Ouyang, S. Yan, Z. Li, T. Yu, Z. Zou, J. Mater. Chem. 21 (2011) 11347–11351.
[35] H. Kim, J. Han, Res. Chem. Intermed. 40 (2014) 2431–2437.
[36] A. Ashkarran, M. Ghavamipour, H. Hamidinezhad, H. Haddadi, Chem. Intermed. 41 (2015) 7299–7311.
[37] H. Kang, S. Park, Int. J. Hydrogen Energy 36 (2011) 9496–9501.
[38] R. Niishiro, S. Tanaka, A. Kudo, Appl. Catal. B 150–151 (2014) 187–196.
[39] W. Chen, C. Li, H. Gao, J. Yuan, W. Shangguan, J. Su, Y. Sun, Int. J. Hydrogen Energy 37 (2012) 12846–12851.
[40] T. Ishii, H. Kato, A. Kudo, J. Photochem. Photobiol. A: Chem. 163 (2004) 181–186.
[41] W. Chen, B. Yang, Q. Yu, L. Mao, Z. Fan, Q. Wang, W. Shangguan, App. Surf. Sci. 355 (2015) 1069–1074.
[42] D. Wang, J. Ye, T. Kako, T. Kimura, J. Phys. Chem. B 110 (2006) 15824–15830.
[43] X. Zhou, J. Shi, C. Li, J. Phys. Chem. C 115 (2011) 8305–8311.
[44] T. Mishima, M. Matsuda, M. Miyake, Appl. Catal. A: Gen. 324 (2007) 77–82.
[45] D. Hou, X. Hu, W. Ho, P. Hu, Y. Huang, J. Mater. Chem. A 3 (2015) 3935–3943.
[46] K. Maeda, M. Higashi, D. Lu, R. Abe, K. Domen, J. Am. Chem. Soc. 132 (2010) 5858–5868.
[47] D. Barreca, G. Carraro, V. Gombac, A. Gasparotto, C. Maccato, P. Fornasiero, E. Tondello, Adv. Funct. Mater. 21 (2011) 2611–2623.
[48] K. Maeda, K. Teramura, D. Lu, T. Takata, N. Saito, Y. Inoue, K. Domen, J. Phys. Chem. B 110 (2006) 13753–13758.
[49] K. Maeda, H. Terashima, K. Kase, M. Higashi, M. Tabata, K. Domen, Bull. Chem. Soc. Jpn. 81 (8) (2008) 927–937.
[50] Y. Yuan, Z. Zhao, J. Zheng, M. Yang, L. Qiu, Z. Li, Z. Zou, J. Mater. Chem. 20 (2010) 6772–6779.
[51] R. Abe, K. Sayama, H. Sugihara, J. Phys. Chem. B 109 (2005) 16052–16061.